Planck Polarimetry: Modeling the Galactic Magnetic Field

A THESIS SUBMITTED TO THE FACULTY OF THE GRADUATE SCHOOL
OF THE UNIVERSITY OF MINNESOTA
BY

Theodore Park Wahl

IN PARTIAL FULFILLMENT OF THE REQUIREMENTS
FOR THE DEGREE OF
MASTER OF SCIENCE

Terry J. Jones, Advisor

June 2010

Acknowledgements

I want to thank and acknowledge the tireless efforts of my advisor, Terry Jones. Without him I would not have been able to do this. I would like to thank him for his guidance in this project and support while writing this thesis.

I also want to acknowledge my fellow graduate students, who have been an immense support during my time here. No student gets through graduate school without help, and I am no different. Thanks guys.

Dedication

This thesis is dedicated to my parents, Russell Wahl and Pamela Park.

Planck Polarimetry: Modeling the Galactic Magnetic Field

by Theodore Park Wahl

Under the supervision of Terry J. Jones

Abstract

I created a model of polarized emission from dust grains aligned with the galactic magnetic field for comparison with Planck observations. I modeled the magnetic field in the galactic disk as a field with a cylindrical constant component and an equal strength random component. I investigated how the fractional polarization down a line of sight varies with different models of a random field. I determine that different models of random fields yield different amounts of fractional polarization, especially over sightlines longer than a decorrelation length.

Table of Contents

List of Figures

Chapter 1

Introduction

The goal of my research project was to create synthetic observations of polarized emission from dust grains in the disk of the galaxy. The impetus of this project was the launching of the Planck mission. Planck's primary goal is to observe the CMB, but it is also sensitive to polarization and frequencies where emission from dust grains contributes to the overall signal. This allows Planck to observe the polarized dust emission in the galactic disc.

Because we know that polarization due to dust delineates the magnetic field geometry of the galaxy, observations and analysis of the polarized emission will reveal the geometry of the field. Before that can be accomplished, we need a way of understanding what various magnetic field configurations will look like from Earth's vantage point in the galaxy. This is what my program does. It takes in a user specified field configuration, calculates the resulting polarization along a line of sight, and displays the results for the entire galactic disk.

The majority of my time on this project was spent in creating this projection and propagation computer program and then in creating a viable random field geometry. As will be shown in Chapter 2, previous observations reveal that the magnetic geometry of the galactic disk is dominated by two components: a cylindrical constant component and a random component. For my project I used both components, based on the observations

and analysis done by Jones et al. (1992) The other major part of my project was testing different techniques for generating the random component of the magnetic field. As will be discussed in Chapter 4 this test is important for understanding the effect the random component has on the model results.

Chapter 2

Background

By comparing the polarization from dust with other effects which respond to magnetic fields it is easy to show that dust polarization can delineate galactic magnetic fields. An example of this is shown in Figure 2.1 where H band polarization and 6.2 cm synchrotron polarization from NGC 891 are displayed. The H band polarization comes from dust grains polarizing background light. If these grains are aligned with that galaxy's magnetic field, their polarization vectors should be perpendicular to the synchrotron polarization vectors. This is what is observed; confirming that polarization due to dust delineates galactic magnetic fields.

There are two ways aligned dust grains can polarize light: One, because the grains are non-spherical they can act as a polarizing filter to background starlight. Two, the aligned non-spherical grains also emit polarized radiation. Figure 2.2 illustrates the two processes. Observers can then indirectly observe the magnetic field geometry by observing this polarized light. Because Planck will measure the polarized emission of dust in the galactic plane I will be focusing on this mechanism in this chapter.

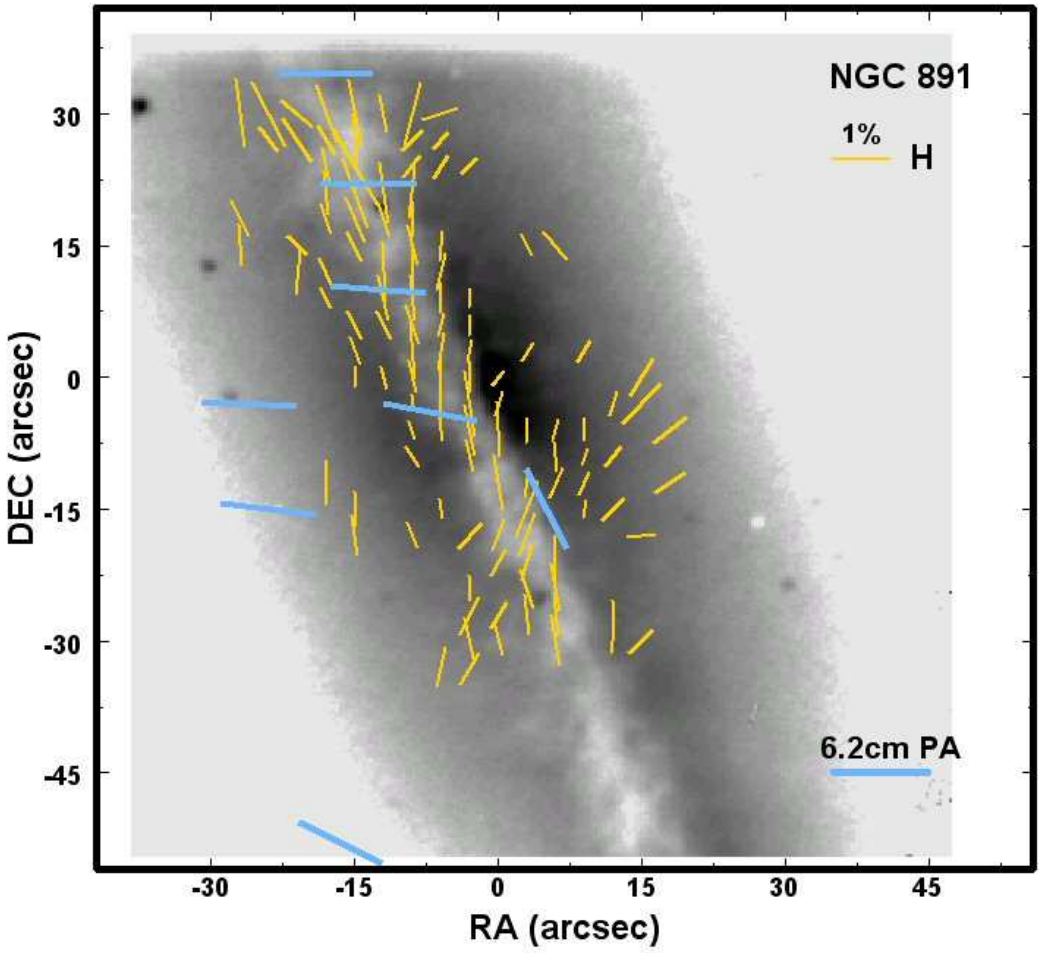

Figure 2.1. NGC 891 with yellow vectors representing polarization measurements in the H band and blue vectors representing 6.2 cm radio synchrotron polarization from Sukumar and Allen. The polarization in the H band comes from dust grains acting as a polarizing filter. If both are measuring the same field they are expected to be perpendicular. (Source: T. J. Jones)

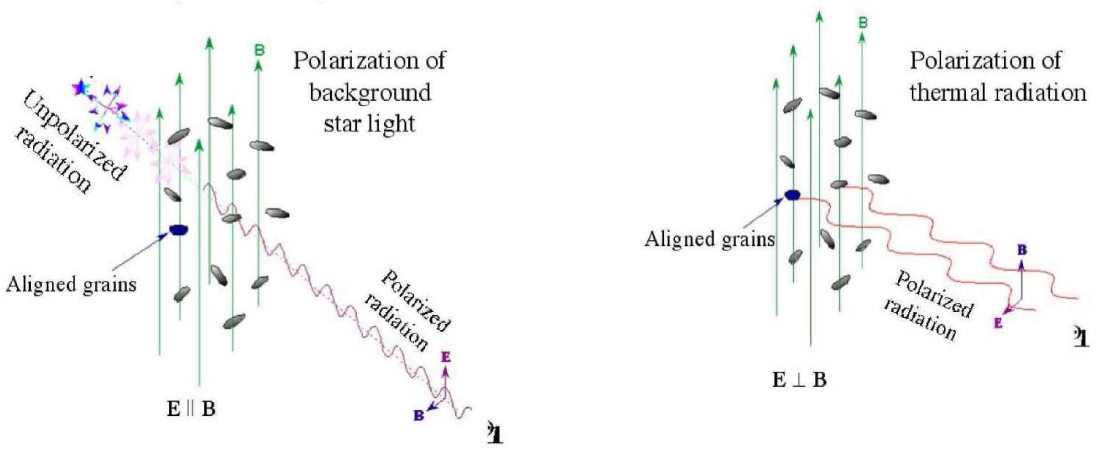

Figure 2.2. Polarization due to dust. *(a)Left panel*- Showing the polarization of starlight through aligned dust grains. The direction of polarization (**E**) is parallel to the magnetic field direction in the plane of the sky. *(b)Right panel*- Showing the emission of polarized radiation from aligned dust grains. The direction of polarization is perpendicular to the magnetic field direction in the plane of the sky. (Source: Lazarian 2008)

The dust grains are routinely modeled as ellipsoids and the grains are somehow aligned with their long axes perpendicular to the magnetic field. The precise process of alignment is still not completely understood, however there are numerous theories attempting to explain this behavior. It is easy to see how these grains can polarize background light: they preferentially absorb starlight along their long axes. The physics for polarization in emission are equally simple; the "warm" grains emit thermal radiation and the component along the longer axis is therefore greater.

Draine and Lazarian in their 1999 paper review the three main methods by which dust grains can emit radiation. The most powerful is thermal emission: thermal fluctuations in the charge distribution of the grain cause it to emit dipole radiation. The radiation from this process peaks in the far infrared at $\lambda \sim 100\mu m$ as is expected for grains that are at temperatures of tens of Kelvins. The second method is magnetic dipole emission due to thermal fluctuations in the magnetization of the material. If the grains contain magnetic material this has the possibility of being a strong contribution. However, because the ferromagnetic content of interstellar dust grains is not known to be high this effect can be ignored. The third is rotational electric dipole emission caused by the rotating electric dipole moment of the spinning grain. This emits at much lower frequencies and is therefore outside the interests of my project.

Each grain emits polarized radiation individually, but the effect only becomes noticeable when they are aligned with a magnetic field. To create synthetic observations of what Planck will observe in the Galactic disk I had to create a plausible model for the magnetic field in the Galactic disk. Working from Jones 1989 and Jones, Klebe & Dickey

1992 I decided to model a field that had a cylindrical (constant) component and a random component.

Using the results of earlier rotation measure studies of pulsars and extragalactic sources, Zeeman effect surveys in the 21 cm line, and studies of the polarization of the low-frequency galactic non-thermal background; Jones et al. suggested the general geometry of the magnetic field was of cylindrical shape in the galactic plane. For simplicity, and because I am concerned with the galactic plane only, I have ignored the effects of the spiral arms. This cylindrical field will be the constant component of my model.

The observations also suggest a random component to the field. Working on modeling the polarization of transmitted light, Jones et al. used two different ways of characterizing a random field. One way describes the magnetic field as Alfven waves where the amplitude of the wave determines the extent to which the field direction can fluctuate along a line of sight. The other way describes the random component of the field as a vector, randomly distributed over 4π steradians at each point with the magnitude of the vector having a Gaussian distribution about each rectangular coordinate. This is similar to what Myers and Goodman (1991) did and so Jones et al. refer to it as the “Myers and Goodman model”.

Essentially both descriptions generate a randomly pointing vector at each measuring point along a line of sight; this is shown in figure 2.3. This description is known to be un-physical because it describes a magnetic field that may diverge, but is useful as an approximation. Both descriptions involve the path length over which this

random field is no longer correlated; i.e. the decorrelation length. Both descriptions of the random component yielded similar results.

The main conclusions of Jones et al. were: One, that the trend in polarization with extinction at 2.2 μm can be well modeled by assuming there is no dependence of the polarization on field strength and that the large elongated dust grains are maximally aligned. The factors influencing the magnitude of the polarization are the column density of dust and the magnetic field direction along the line of sight. Two, that the observed dispersions in polarization magnitude and position angle are best modeled by a field with equal strength steady and random components. This is demonstrated in figure 2.4. Three, the decorrelation length must be tied to the optical depth—the column density—not the physical path length. The authors determined that the value of the decorrelation length must be narrowly distributed around 500 parsecs in the diffuse interstellar medium. (Jones et al. 1992)

One of the missions that will be observing this polarized dust radiation is Planck. It is a space telescope launched and run by the ESA. It is currently orbiting the Earth-Sun L2 point as it images the entire sky. Its primary mission is to observe the fluctuations of the Cosmic Microwave Background and it will also be able to measure the polarization of the CMB. Planck contains nine separate detectors with center frequencies of 30, 44, 70, 100, 143, 217, 353, 545, and 857 GHz. In the process of observing the CMB Planck will of course also image the entire Galaxy. For its three highest frequency bands, the emission from dust is a significant contribution to the total signal. The 353 GHz channel

is sensitive to polarization and has an angular resolution of 5 arcminutes. This allows Planck to observe the polarized emission from dust for the entire galaxy in great detail.

The polarized emission from dust will delineate the Galactic magnetic field. So Planck is, almost unintentionally, well situated to investigate the Galaxy's magnetic geometry. In the next chapter I will discuss how I created synthetic polarization maps with the goal of providing a comparison to what Planck observes.

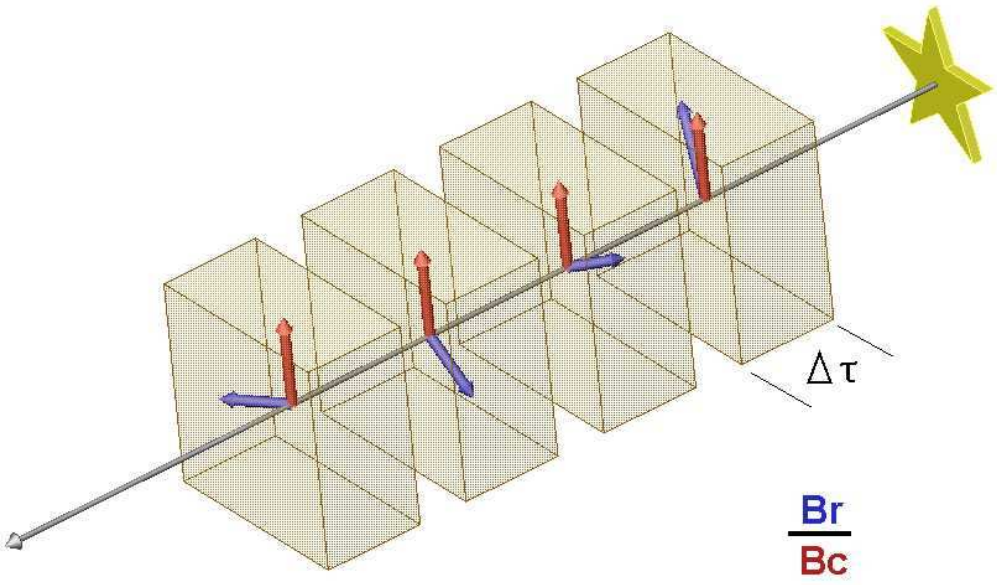

Figure 2.3. Schematic representation of the two input parameters to the JKD model. Delta Tau is the optical depth of a single cell in which the net magnetic field geometry is single valued; this corresponds to what I call the decorellation length. Br/Bc is the ratio of the random (blue vectors) to constant (red vectors) components of the magnetic field. The random component changes at each step in Delta Tau. (Source: T. J. Jones.)

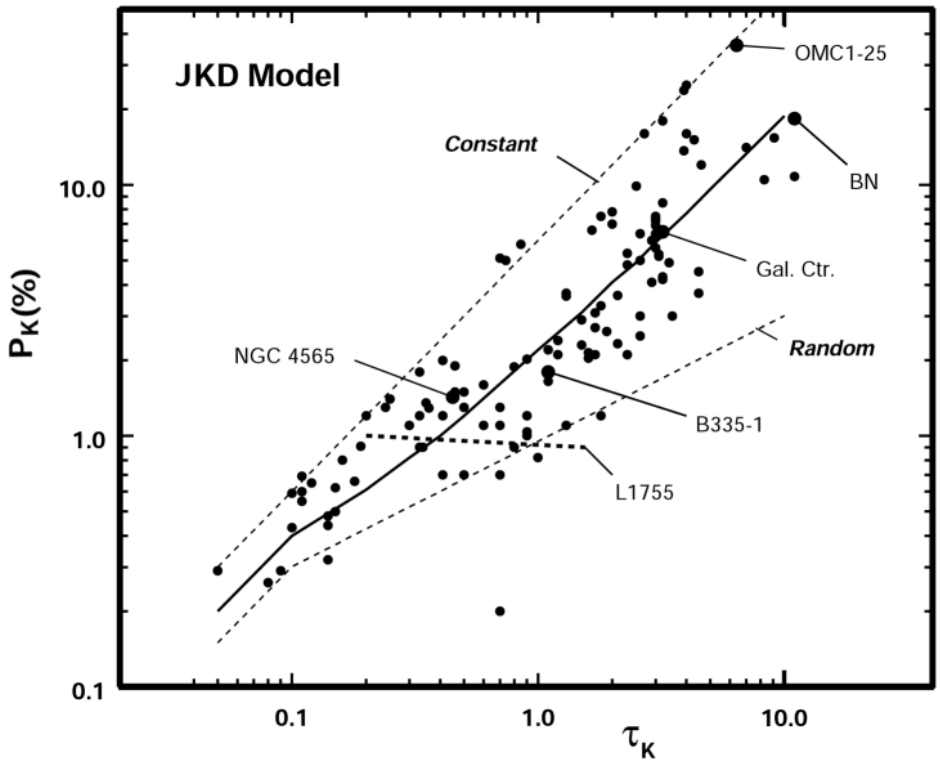

Figure 2.4. K (2.2 μm) band percent polarization versus optical depth. The dots are data from Jones 1989. The upper dotted line represents the results for a constant magnetic field. The lower dotted line represents a purely random magnetic field. The solid line represents a model with equal strengths in the random and constant components. All lines are for a $\Delta\tau = 0.1$ which corresponds to a decorrelation length of 500 pc. (Source: T. J. Jones)

Chapter 3

Making the Model

My first task was to create the magnetic field. I used a Cartesian grid of points with the galactic center at the origin. The Earth's position was at (0, 80, 0) meaning that in my grid a distance of 1 corresponds to 100 parsecs. A diagram of the coordinate system and constant field is shown in figure 3.1. The constant field is a purely cylindrical field whose direction was based on the point of interest's location.

$$\begin{aligned} B_{0,x} &= \frac{-y}{\sqrt{x^2+y^2}} \\ B_{0,y} &= \frac{x}{\sqrt{x^2+y^2}} \\ B_{0,z} &= 0 \end{aligned} \tag{3.1}$$

As can be seen in equation 3.1, the x and y components of the steady field are engineered to create cylindrically pointing unit vectors while the z component is zero.

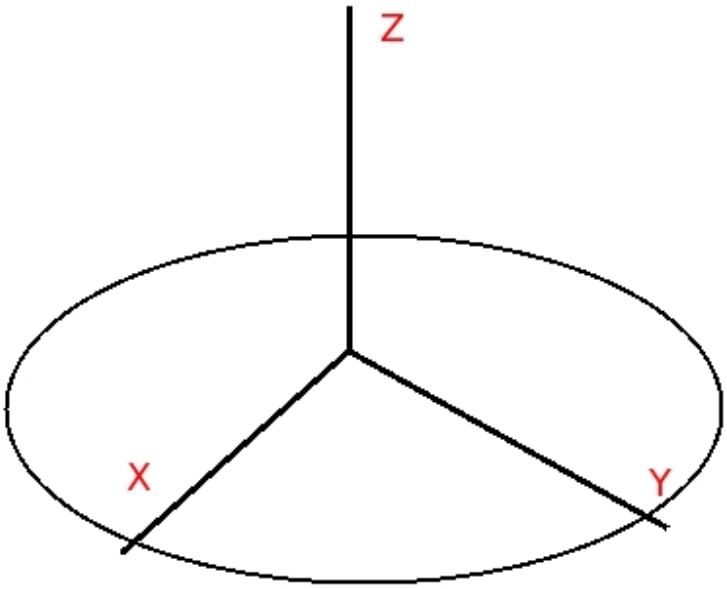

Figure 3.1. Diagram of constant component and coordinate system. The circle demonstrates one magnetic field line in the cylindrical geometry of the constant component. The galactic center is at the origin, and the Sun is on the y-axis.

The creation of the random field is more complex. The simplest solution would be to add in a randomly pointing vector at each point, and this was done by Jones et al. as their Myers and Goodman model. I call this the simple random model and will use it in Chapter 4 for testing purposes. However, this is not an accurate physical model because it does not obey one of Maxwell's laws, the requirement that the magnetic field be divergence free:

$$\nabla \cdot \vec{B} = 0 .$$

There are numerous ways to represent a random field that does obey this law. For my simulation I used an approach developed by Giacalone and Jokipii (1999). Again, the random field is represented by a vector unique to each point.

$$\overrightarrow{\delta B} = \sum_{n=1}^{N} A_n \overrightarrow{\xi_n} \sin\left(k_n z' + \beta_n\right) \tag{3.2}$$

The random vector is a sum of N separate vectors each constructed like so:

$$\overrightarrow{\xi_n} = \cos\left(\alpha_n\right)\hat{x}_n' + \sin\left(\alpha_n\right)\hat{y}_n' \tag{3.3}$$

The primed directions come from a rotation through random angles unique to each "n" value.

$$\begin{pmatrix} x_n' \\ y_n' \\ z_n' \end{pmatrix} = \begin{pmatrix} \cos(\theta_n)\cos(\phi_n) & \cos(\theta_n)\sin(\phi_n) & -\sin(\theta_n) \\ -\sin(\phi_n) & \cos(\phi_n) & 0 \\ \sin(\theta_n)\cos(\phi_n) & \sin(\theta_n)\sin(\phi_n) & \cos(\theta_n) \end{pmatrix} \begin{pmatrix} x \\ y \\ z \end{pmatrix} \tag{3.4}$$

The angles α_n, β_n, θ_n, and φ_n are random numbers between 0 and 2π. This creates a global field that obeys the divergence free requirement, and as the number of separate vectors increases the more this behaves like the simple random model. The decorrelation length of the magnetic field is related to the value of k_n. This can be thought of as a wave

number with the desired decorrelation length corresponding to the wavelength; k_n = 2π/decorellation length. An option Giacalone and Jokipii choose is to have k_n change for each separate vector, whereas I kept k_n constant—equivalent to a constant decorrelation length. The differences in these approaches will be discussed in the next chapter.

To insure that the constant and random components in the model were of equal strength I sought to normalize the random component. I created a test field composed solely of a random component with the desired number of component vectors each with $A_n = 1$. The program measures the magnitude of the random component at $9*10^5$ points in the galaxy and computes the rms average from these measurements. The inverse of this average then became the amplitude of the random constituent vectors used in the model. From point to point the strength of the random component varies, but over the entire galaxy its average strength is now equal to the constant component.

For any desired point the magnetic field vector is the sum of the constant and random components at that point. The next step is to project it into the plane of the sky. This is a simple mathematical operation. The initial magnetic vector at point "i" is given by:

$$\overrightarrow{B_i} = \overrightarrow{B_{0_i}} + \overrightarrow{\delta B_i} \tag{3.5}$$

Based on the conclusions of Jones et al. that the actual strength of the magnetic field was unimportant, and to simplify my calculations, I set the magnitude of every unprojected magnetic vector equal to one; $|\mathbf{B}| = 1$.

I then define $\mathbf{n_i}$ as the vector connecting the point of interest (x_i, y_i, z_i) and Earth. This vector also serves as the normal vector to the plane of the sky at that point. The magnetic field vector projected onto the plane of the sky, $\mathbf{B`_i}$, is given by:

$$\vec{B}_i' = \hat{n}_i \times \left(\vec{B}_i \times \hat{n}_i\right) \tag{3.6}$$

I define the angle between the line of sight and the magnetic field vector to be θ such that θ = 0 is a vector pointing toward us and θ = π/2 is a vector in the plane of the sky. The length of the projected vector is then:

$$B_i' = B_i \sin(\theta) \tag{3.7}$$

The next step is to calculate the Stokes' Q and U values at this point. First, though, the dust density needs to be determined. This is because the volume emission at any point is proportional to the dust density at that point. For my model I used a simple exponential disk to represent the dust distribution in the galaxy:

$$\rho(x_i, y_i, z_i) = \rho_0 e^{-r/\alpha} e^{-z/\beta} \tag{3.8}$$

Here $\rho(x_i,y_i,z_i)$ represents the density of dust at point i. Since I was more concerned with the fractional polarization values than intensities, I simply set $\rho_0 = 1$. The scale length of the disc was set at $\alpha = 4$ kpc and the height at $\beta = 50$ pc. The x and y values of the point determined r; $r = (x_i^2 + y_i^2)^{1/2}$ and of course $z = z_i$. The polarized intensity is:

$$I_p = \rho(x_i, y_i, z_i)\Delta l \left(\frac{B_i'}{B_i}\right)^2 \tag{3.9}$$

Here Δl is the step size along the line of sight. For all my calculations I set Δl = 1 pc. The projected electric vector goes as sin(θ) and intensity goes as the electric vector squared,

so the polarized emission from the dust grains goes as $\sin^2(\theta)$ which is equivalent to $(B`/B)^2$.

Now Stokes' Q and U are found through:

$$\begin{aligned} Q_i &= I_p \cos(2\psi_i) \\ U_i &= I_p \sin(2\psi_i) \end{aligned} \tag{3.10}$$

Where "ψ_i" is the angle between the projected magnetic field and Galactic north projected into the plane of the sky at that point, measured east of north.

The next phase of the program looks down a line of sight calculating the integrated Stokes Q and U vectors and the integrated intensity. Because we are investigating the diffuse interstellar medium and simulating emission at 353 GHz, we can assume the optically thin case. This greatly simplifies the calculations; at each step along a line of sight the Stokes Q and U vectors add to the previous step's values. So for N steps the final Q, U and intensity I are:

$$\begin{aligned} Q &= \sum_{i=1}^{N} Q_i \\ U &= \sum_{i=1}^{N} U_i \\ I &= \sum_{i=1}^{N} \rho(x_i, y_i, z_i)\Delta l \end{aligned} \tag{3.11}$$

The total fractional polarization for a desired line of sight is then found from the following calculation:

$$P = \frac{\sqrt{Q^2 + U^2}}{I} \tag{3.12}$$

With the ability to look down any line of sight the next task was to create a map of the galactic disc as seen from the Earth. I set the limit on the size of the galaxy as a disc of radius = 31 kpc and a thickness of 1 kpc. With the decreasing exponential model of dust density used in the program it was decided that these values were sufficiently large enough to ensure accuracy. The program calculates the fractional polarization along a line of sight until reaching the edge and then starts on a different galactic longitude and latitude.

Figure 3.2 is an example synthetic polarization map of a purely cylindrical magnetic field. The figure displays only a small portion of the galactic disc to illustrate some effects that demonstrate the projection program is working as expected. At galactic latitude, *b*, of 0^0 we see polarization with an angle of 90^0 to north which is expected from the cylindrical field. At longitude, *l*, of 30^0 and greater, as latitude increases we see a trend of the fractional polarization increasing. This is because as the latitude of the line of sight increases more of the magnetic field vector is being projected into the plane of the sky—increasing the polarization. The final effect is evident at around $l = 90^0$ where the length of the polarization vectors drop almost to zero; this is where the magnetic field is almost entirely perpendicular to the plane of the sky. This shows that the program is calculating the magnetic field correctly, projecting the field correctly, and is calculating the polarization correctly.

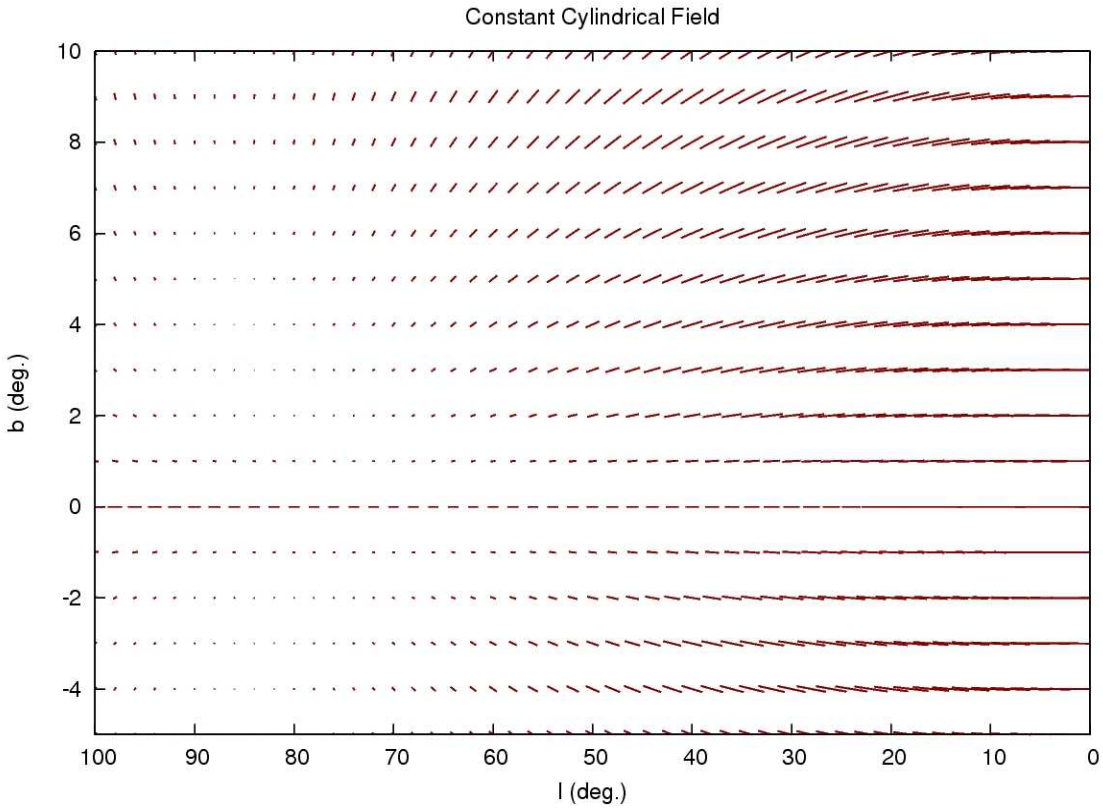

Figure 3.2. This shows an example map of a portion of the galactic disc for a purely cylindrical magnetic field. The axes are the galactic longitude, *l*, and latitude, *b*, in degrees. The vectors represent the polarization of that particular line of sight; the angle of the vector represents the angle of polarization and the length of the vector represents fractional polarization.

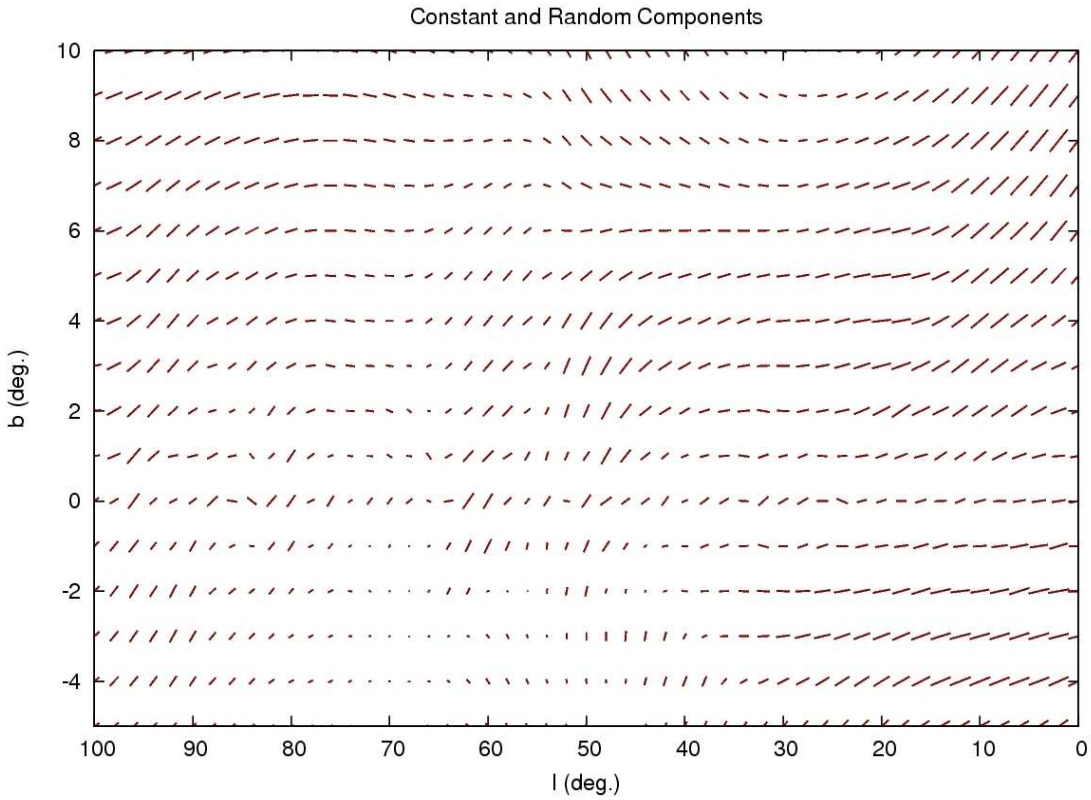

Figure 3.3. This shows an example map of a portion of the galactic disc for a constant and random magnetic field of 20 units with a decorrelation length of 500 parsecs. The axes are the galactic longitude, *l*, and latitude, *b*, in degrees. The vectors represent the polarization of that particular line of sight; the angle of the vector represents the angle of polarization and the length of the vector represents fractional polarization.

Figure 3.3 shows the map of a 50/50 combination of a cylindrical component and a single realization of a random component composed of 20 smaller vectors each with a decorrelation length of 500 parsecs. Comparing figure 3.3 and figure 3.2 we can see that there are several differences; all due to the addition of the random component. For example: In figure 3.2 around longitude 0^0 all the vectors are at 90^0 from north. In figure 3.3 in the same locations the vectors exist at a range of angles. Another example: in figure 3.2 around longitude 80^0-90^0 the fractional polarization is very low whereas in figure 3.3 it is larger.

What is surprising is how strong the effects of the random component appear to be. They seem to dominate the observed polarization pattern. An explanation could be that because of the influence of the density variations along a line of sight, areas with a strong random component outweigh the other areas of cylindrical field. The next stage of my project was to investigate the behavior of this random component.

Chapter 4

Analyzing the Random Field

In order to investigate the behavior of this random component I wanted to determine how the fractional polarization changes down a single line of sight with the inclusion of only a random field. I wrote a modified version of the program so that it contained only the random component, calculated the fractional polarization along a single line of sight, and measured the fraction polarization accumulated at each step. The density was held constant. To get a statistical average I ran each test 1000 times with different random seeds each time.

An additional motivation was to determine whether a random field composed of varying decorrelation lengths as used by Giacalone & Jokipii or a random field with a constant decorrelation length as used by myself behaved similarly to the simple random model. Some effort was also put into determining if these methods were producing the expected initial fractional polarization values for very short distances, i.e. before a decorrelation length has been traversed.

We can compute this initial polarization from first principles. It is equivalent to finding the average length of a randomly pointing unit vector projected onto the plane of the sky. If the angle separating the line of sight and the random vector is θ, then the length of the projected vector is $\sin(\theta)$. The probability of any individual angle being chosen is $2\pi \sin(\theta)$, so the average length can be found through:

$$\mu = \frac{2\pi\int_0^{\pi} \sin(\theta)^2 d\theta}{2\pi\int_0^{\pi} \sin(\theta) d\theta} = \frac{\pi}{4} \approx 0.785 \tag{4.1}$$

This is the average fractional polarization we expect for the first step. A similar calculation can be done to produce the standard deviation for this mean fractional polarization value:

$$\sigma = \sqrt{\frac{2\pi\int_0^{\pi} \left(\sin(\theta) - \frac{\pi}{4}\right)^2 \sin(\theta) d\theta}{2\pi\int_0^{\pi} \sin(\theta) d\theta}} \approx 0.223 \tag{4.2}$$

Figures 4.1 through 4.3 show the fractional polarization as a function of distance down a line of sight for each of the models. The expected initial fractional polarization is displayed as a green x on each of the figures, and all models are in close agreement with this value.

Figure 4.1 displays the polarization results for the simple model of a randomly pointing vector at each measurement point. It was expected to behave similarly to a random walk in the Q and U plane. The fractional polarization would decrease with the square root of the number of steps taken. This is the observed behavior.

Figure 4.2 displays the polarization for the random model used in the synthetic polarization map making program. Its construction is detailed in equations 3.2 – 3.4 and it has a constant decorrelation length of 500 pc. Figure 4.3 displays the results for a random model constructed the same way but with varying decorrelation lengths. This is similar to the way Giacalone and Jokipii (1999) constructed their model of a random field. It has a maximum length scale of 500 pc and the components with shorter

decorrelation lengths follow a Kolmogorov spectrum in amplitude. The decorrelation length for the n-th component, $\lambda_{n,}$ is given by:

$$\lambda_n = \frac{500\,pc}{500^{\frac{n-1}{N-1}}} \tag{4.3}$$

Here N is the total number of components used in the random field (see eq. 3.2).

Comparing figures 4.2 and 4.2, we can see that both produce similar values at very short (less than one decorrelation length) distances. However, at greater distances they exhibit different behavior. The variable decorrelation length model drops faster and then approaches a constant value. This can be attributed to the effects of the smaller length scales. The constant decorrelation length model in figure 4.2 more closely follows the results of the simple random model. All three models are shown together in figure 4.4.

All three models start at similar fractional polarization values. As expected. It is at larger distances that their behaviors vary. There is a pronounced difference between the constant and variable decorrelation length models—the models designed to represent magnetic fields that are divergence free. This shows that different models of the random magnetic field will yield different synthetic polarization maps for comparison with Planck. These differences will be most noticeable over long to intermediate sight lines, where there are more decorrelation lengths.

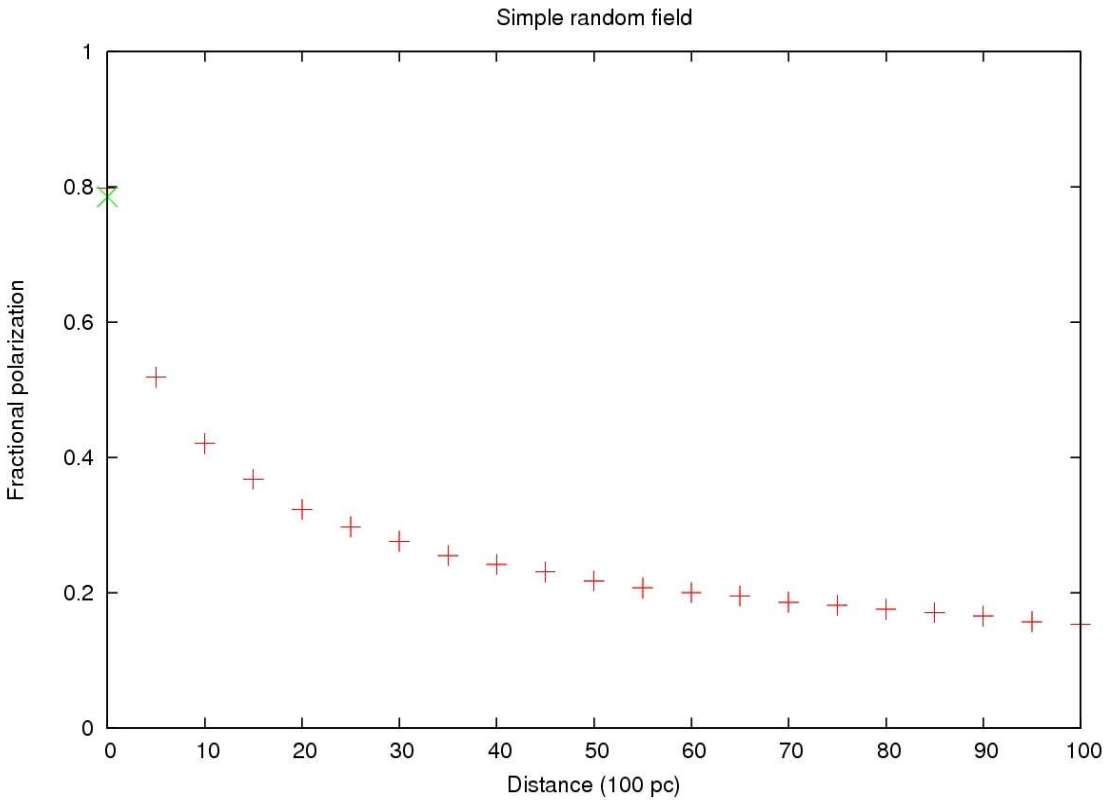

Figure 4.1. The red points show the computed fractional polarization down a line of sight for the simple random model composed of a randomly pointing vector at each point. The green x represents the expected average initial fractional polarization (see eq. 4.1). Each point is separated by 500 pc.

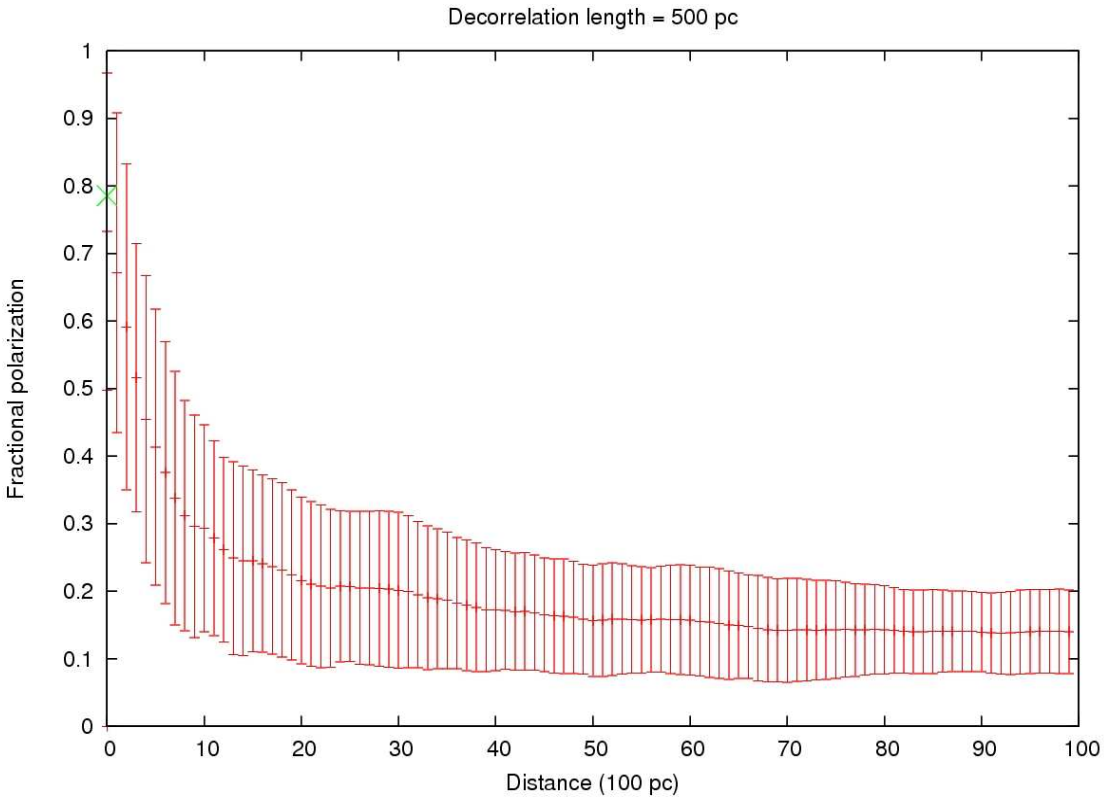

Figure 4.2. This shows the computed fractional polarization down a line of sight for a random field composed of 100 components with constant decorrelation length of 500 pc. The bars represent the standard deviation of the fractional polarization from 1000 realizations. This is in agreement with eq. 4.2. The green x represents the expected average initial fractional polarization (see eq. 4.1).

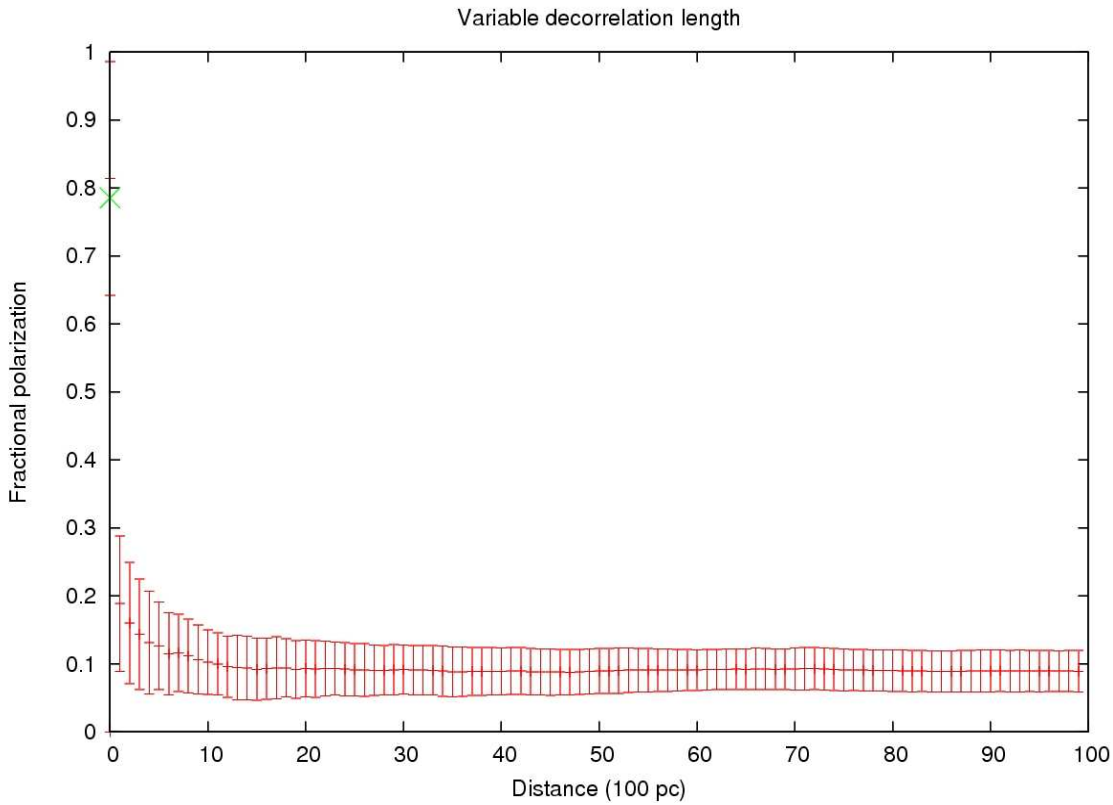

Figure 4.3. This shows the resulting fractional polarization down a line of sight for a random field composed of 100 components with variable decorrelation lengths—maximum of 500 pc. The bars represent the standard deviation of the fractional polarization from 1000 realizations. This is in agreement with eq. 4.2. The green x represents the expected average initial fractional polarization (see eq. 4.1).

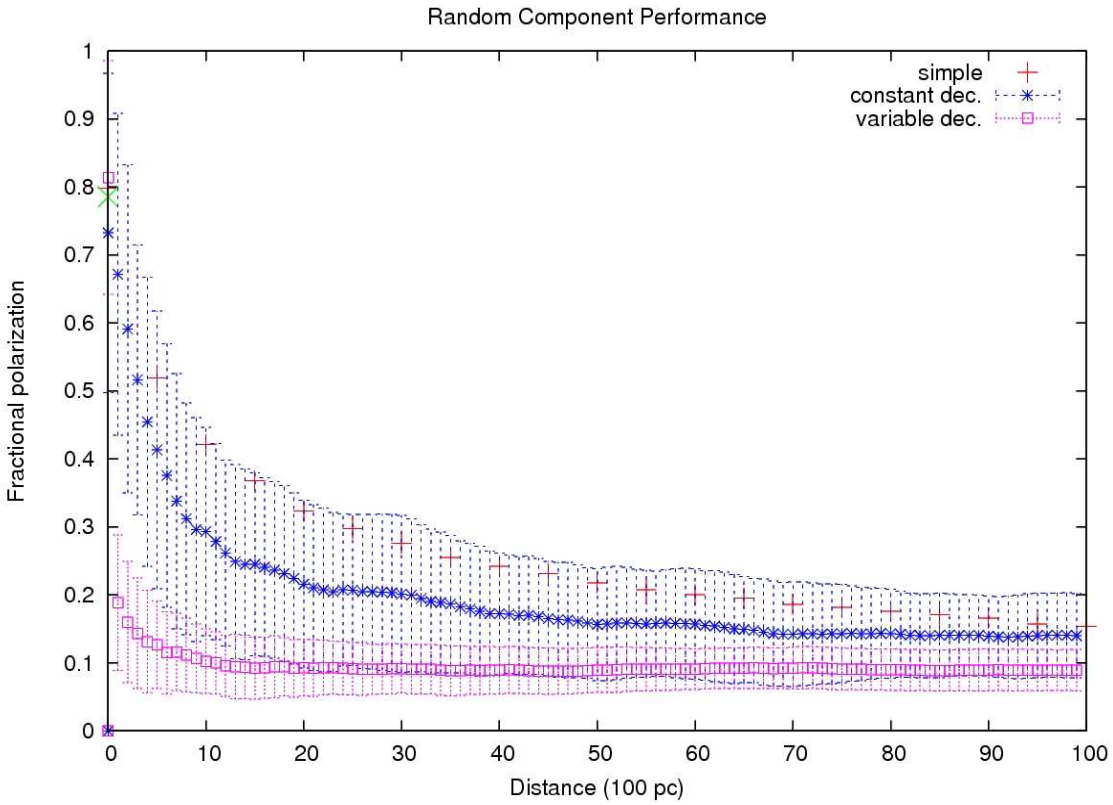

Figure 4.4. All three random field model's fractional polarization. The simple random field is represented in red, the variable decorrelation length field is represented in purple, the constant decorrelation length field is blue. The bars represent the standard deviation of the fractional polarization from 1000 realizations. This is in agreement with eq. 4.2. The green x represents the expected average initial fractional polarization (see eq. 4.1).

Chapter 5

Conclusions

I was able to create synthetic observations of the polarized emission from dust grains aligned with a model magnetic field. My results show that including a random component can dramatically change what the observer sees. With an equal weight between constant and random components to the magnetic field, the random component obviously dominates in certain areas. The method of creating the random field also matters. As shown in Chapter 4, the different random fields yielded different amounts of fractional polarization over intermediate distances.

References

Draine, B. & Lazarian, A. 1999, *ASP Conference Series*, **181**, 133.

Giacalone, J. & Jokipii, J. R. 1999, *ApJ*, **520**, 204.

Jones, T.J. 1989, *ApJ*, **346**, 728

Jones, T.J., Klebe, D., Dickey, J. 1992, *ApJ*, **389**, 602

Lazarian, A. 2008, arXiv:0811.1020v1.

Myers, P.C. & Goodman, A.A. 1991, *ApJ*, **373**, 509.